ELSEVIER

Journal of Non-Crystalline Solids 208 (1996) 56–63

JOURNAL OF NON-CRYSTALLINE SOLIDS

Spectral properties of Er^{3+}-doped gallium lanthanum sulphide glass

C.C. Ye, D.W. Hewak, M. Hempstead *, B.N. Samson, D.N. Payne

Optoelectronics Research Centre, University of Southampton, Southampton SO17 1BJ, England, UK

Received 23 October 1995; revised 14 November 1995

Abstract

The spectral properties of chalcogenide glass $0.7Ga_2S_3{:}0.3La_2S_3$ (Ga:La:S) doped with Er^{3+} are presented and discussed. Emission and absorption spectra and lifetimes of energy levels have been measured. The 2.7 μm emission of Er^{3+} has been observed from chalcogenide glass for the first time. Radiative and non-radiative transition rates are calculated and compared with the measured lifetimes of interesting energy levels. Comparing this glass with Er^{3+}-doped silica glasses, it is shown that the absorption and emission cross-sections of Er^{3+}-doped Ga:La:S are around 2.5 times higher, radiative transition rates are around five times higher due to its higher refractive index, while multiphonon non-radiative decay rates are around three orders lower due to its much lower phonon energy. Furthermore, the inverse energy transfer process in Er^{3+}:Ga:La:S glass may have significant implications for the operation of Er^{3+}:Ga:La:S devices. These spectral properties, along with the higher solubility for rare earth-ions in Ga:La:S, make this glass a good candidate for new applications.

1. Introduction

Rare-earth-doped chalcogenide glasses are of considerable interest, most recently for the role they play as hosts for efficient 1.3 μm optical fibre amplifiers [1]. In particular, high fluorescence efficiency of Pr^{3+}-doped gallium–lanthanum sulphide (Ga:La:S) glass has been demonstrated theoretically and experimentally and efforts are underway to realize this glass in optical fibre form [2–4].

In addition, Ga:La:S glass offers other advantages. The rare-earth ion, through substitution for the lanthanum ion, occupies a well-defined site within the glass matrix and allows very high dopant concentrations to be obtained without concern for ion-clustering [5]. High solubility for rare-earths, along with the low phonon energy and high refractive index make the glass doped with erbium a good candidate for new applications, including short fibre amplifiers operating at 1.54 μm, long-wavelength (e.g., 2.7 μm) lasers, 980 nm upconversion lasers pumped at 1.48 μm, and saturable absorbers.

It is well known that the successful development of Er^{3+}-doped silica-based amplifiers operating in the third telecommunication window at 1.54 μm [6] has produced revolutionary changes in communication technology. However the development of silica-based, short fibre amplifiers and planar wave-guide amplifiers has suffered from concentration quenching due to Er^{3+} ion cooperative upconversion [7], which limits the Er^{3+} concentration to a very low level if efficient operation is desired. For various reasons, such as packaging, reduction of internal

* Corresponding author. Tel.: +44-1703 592 809; fax: +44-1703 593 149; e-mail: mh2@orc.soton.ac.uk.

PII S0022-3093(96)00203-7

Rayleigh backscatter and for development of compact, environmentally stable, high-repetition-rate short-pulse lasers, it is desirable to use short fibres with higher Er^{3+} concentration. In addition, Er^{3+}-doped planar waveguide amplifiers must of necessity be short to overcome the high inherent propagation losses. In order to show the possible advantages of Er^{3+}-doped Ga:La:S glass as a host for short amplifiers operating at 1.54 μm, the properties of Er^{3+}-doped Ga:La:S glass are compared with those of Er^{3+}-doped silicate glasses.

Early work on Ga:La:S glasses doped with Er^{3+}, Ho^{3+} and Nd^{3+} was reported by Reisfeld [8]. We have built on this work through an improved glass melting procedure and high purity starting materials, and report here on the full spectral properties of Er^{3+}-doped Ga:La:S.

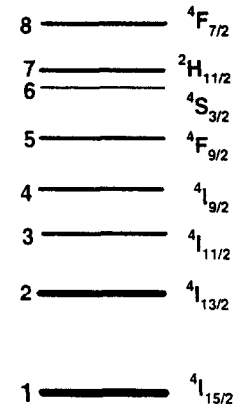

Fig. 1. Energy levels of Er^{3+}.

2. Experimental

2.1. Glass melting

Glasses were prepared in the molar composition 70% Ga_2S_3 and 30% La_2S_3 by melt-quenching the sulphides in a vitreous carbon crucible in a silica ampoule. Typically 100 g melts were fabricated for the spectroscopic evaluation described in this paper. The erbium dopant concentrations for the two bulk samples used for this paper are 0.0158 mol% (LD143) and 1.58 mol% Er_2S_3 (LD154), respectively.

Both Ga_2S_3 and La_2S_3 starting materials were provided by Merck who manufacture their sulphides through a proprietary process which insures contamination by oxides is typically less than 1%. This differs from other commercially available sulphides where contamination levels of up to 5% have been measured.

2.2. Absorption spectrum

Energy levels of the Er^{3+} ion are shown in Fig. 1. The absorption spectrum of a sample LD154 was measured using a Lambda spectrometer over a range of 400–3200 nm. Identical results were obtained in different regions of the sample, indicating that the erbium ions in the sample are macroscopically uniformly distributed. Due to the strong electronic absorption at short wavelength (the Urbach edge is 530 nm), there are only five observable absorption bands.

2.3. Emission spectra

The bulk sample was polished on three faces, and the fluorescence was collected from the side ensuring a short path through the glass to avoid significant reabsorption. The 1.54 μm emission and upconversion emission spectra were obtained with an ANDO spectral analyzer. The 2.7 μm emission from $^4I_{11/2}$ to $^4I_{13/2}$ was observed using a Fourier transform spectrometer (Perkin–Elmer System 2000 FT-IR), when the highly-doped sample (LD154) was pumped at 974 nm. The fluorescence was detected by an InSb detector operating at a temperature of −196°C.

2.4. Energy level lifetimes

The ratios of the lifetimes of higher-lying energy levels to that of the first excited level ($^4I_{13/2}$) are expected to be much higher for erbium ions in Ga:La:S than in silica. Consequently, a wide variety of mechanisms may affect the measured fluorescence lifetime of Er^{3+}-doped Ga:La:S. Noting that the measured fluorescence lifetime depends on pumping-conditions and may be very different from the lifetime of the corresponding upper energy level, we chose the pump wavelength, power, and pulse-width carefully. The pump sources were a Ti:Sapphire laser at ~ 800 nm, a dye laser at ~ 650 nm, and laser diodes at 1480 and 974 nm. The pump light

was pulsed with an acousto-optic modulator or a mechanical chopper. The side emission signal was detected through filters; a monochromator was used only when necessary for adequate discrimination of fluorescence power. The detectors used were Hamamatsu Module C5460 Ge or Si APDs, and a photomultiplier. Finally the signal was averaged and recorded using a TEK2232 digital storage oscilloscope. The overall time-resolution, determined by fall-time of the pump pulse, is between a few microseconds and a few tens of microseconds. To avoid concentration effects, the low Er^{3+}-doped sample (LD143) was used in the following lifetime measurements unless indicated otherwise.

The lifetime of the $^4I_{11/2}$ level, τ_3, was determined by measuring 980 nm band fluorescence decay when the sample was pumped at 974 nm using a pulse of width of 40 μs. The pump power was around 50 mW over a light spot diameter of around 0.15 mm.

The lifetime of the $^4I_{13/2}$ level, τ_2. When the sample is pumped at 974 nm, the 1.54 μm fluorescence decay time constant is measured to be 3.0 ± 0.1 ms which must differ from the intrinsic lifetime of the $^4I_{13/2}$ level since the lifetime of the $^4I_{11/2}$ level, τ_3, is comparable to τ_2. Fitting the solution of the ion population rate equations to the measured decay process, we find $\tau_2 = 2.3 \pm 0.1$ ms.

As an alternative approach we have measured the 1.54 μm fluorescence from the highly doped sample pumped at 1480 nm. The pump pulse has a 1.45 ms pulse width, and a power of 45 mW, the light spot diameter being around 0.15 mm. The fitted exponential decay time constant of the 1.5 μm fluorescence is 2.39 ± 0.08 ms. Since only a limited power was available from the 1480 nm laser diode, the dependence of the lifetime on the pump power has not yet been measured. Noting that the $^4I_{11/2}$ level and $^4I_{9/2}$ level have relatively long lifetimes and that a significant ion population can therefore be built up during the pumping process when high pump power is used, the lifetime of the 1.54 μm fluorescence is not expected to be shorter at high pump powers.

The lifetime of the $^4I_{9/2}$ level, τ_4, was evaluated by measuring the 800 nm fluorescence from the $^4I_{9/2}$ level when the sample was pumped at 800 nm, and at 658 nm. The pump pulse was as short as 50 μs.

The lifetime of the $^4F_{9/2}$ level, τ_5, was determined by measuring 650 nm band fluorescence when the sample was pumped at 653 nm, and the pump pulse width was 30 μs.

3. Calculation of transition rates

The total rate of a transition is approximately equal to the sum of the electric dipole transition rate R^{ed}, the magnetic dipole transition rate R^{md} and the non-radiative multiphonon transition rate R^{nr}. The radiative quantum efficiency QE_{ij} of a transition from level i to j is defined as the ratio of the radiative decay rate of the transition to the total decay rate of the energy level i:

$$QE_{ij} = \frac{R_{ij}^{ed} + R_{ij}^{md}}{\sum_{k(E_k < E_i)} \left(R_{ik}^{ed} + R_{ik}^{md} + R_{ik}^{nr} \right)}. \tag{1}$$

3.1. Electric dipole transition rate, R^{ed}

Electric dipole transition rates are calculated on the basis of Judd–Ofelt theory [9–11] using the measured absorption spectrum. The values for the reduced matrix elements are taken from reference [11]. Among the five observable absorption bands, only the $^4I_{15/2} \Rightarrow {}^4I_{13/2}$ transition has a magnetic dipole transition with a significant contribution to the total transition rate. The magnetic dipole transition oscillator strength can be written as: $f^{md} = nf^{md\text{-}o}$, where n is the refractive index, and $f^{md\text{-}o}$ is almost host independent [12]. We use $f^{md\text{-}o} = 30.82 \times 10^{-8}$ for the $^4I_{15/2} \Rightarrow {}^4I_{13/2}$ transition [12]. The refractive index of Ga:La:S can be approximately written as: $n = 2.355 + 1.7919 \times 10^4/\lambda^2 + 7.979 \times 10^9/\lambda^4$ (wavelength λ is in nm) [5]. The electric dipole transition oscillator strength $f^{ed} = f - f^{md}$.

Using the calculated J–O parameters, the electric-dipole transition rate is given by

$$R^{ed} = \frac{1}{4\pi\varepsilon_0} \frac{64\pi^4}{3h(2J+1)\lambda^3} \left(\frac{n^2+2}{3} \right)^2 ne^2 \times \sum_{t=2,4,6} \Omega_t U_t, \tag{2}$$

where U_t ($t = 2, 4, 6$) are the reduced matrix elements.

3.2. Magnetic dipole transition rate, R^{md}

As f^{md}/n is almost host independent, the magnetic dipole transition rate can be calculated from

$$R^{md} = \left(\frac{n}{n^{LF}}\right)^3 R^{md\text{-}LF}, \quad (3)$$

where $R^{md\text{-}LF}$ and n^{LF} are respectively the magnetic dipole transition rate and refractive index of LaF_3 in Ref. [13]. Note that the magnetic dipole transition component is considerable only for the emissions $^4I_{13/2} \Rightarrow {}^4I_{15/2}$ (1.54 μm) and $^4I_{11/2} \Rightarrow {}^4I_{13/2}$ (2.7 μm).

3.3. Non-radiative multiphonon transition rate, R^{nr}

The non-radiative multiphonon transition rate, R^{nr}, can be calculated from

$$R^{nr} = B\exp[-\alpha(\Delta E - 2\hbar\omega_{max})], \quad (4)$$

where ΔE is the energy gap between the two energy levels, $\hbar\omega_{max}$ is the maximum phonon energy, and B, α are host-dependent constants. We estimated the non-radiative decay rate using $\hbar\omega_{max} = 425\ cm^{-1}$, $B = 1.26 \times 10^5\ s^{-1}$, $\alpha = 2.9 \times 10^{-3}$ cm for Ga:La:S glass [1].

4. Results

4.1. Absorption spectrum

The absorption spectrum is shown in Fig. 2. The parameters measured here and in earlier work [8] are summarized in Table 1.

4.2. Emission spectra

The emission cross-section spectrum in the third telecommunication window, as shown in Fig. 3, was determined using the measured emission line shape function, with the peak cross-section being scaled by

$$\frac{1}{\tau_2} = \frac{8\pi n^2}{c^2}\int \nu^2 \sigma_{em}\, d\nu. \quad (5)$$

The measured peak emission cross-section at 1538 nm is $15.7 \times 10^{-21}\ cm^2$, which is around 2.5 times higher than the average value for silicate glasses.

When the sample was pumped at 1480 nm, both 1530 and 980 nm fluorescence were observed, as shown in Fig. 4. Upconversion fluorescence at 980 nm results from energy transfer between two ions in the $^4I_{11/2}$ level. The relative fluorescence power in the two bands depends on the pumping intensity and energy transfer upconversion constant. Fig. 5 shows the recorded decay of 980 nm upconversion fluorescence, as well as the 1480 nm pump pulse trace, which has 0.42 ms width, 10 μs fall time, and pump power of 45 mW. As expected, there is a time delay,

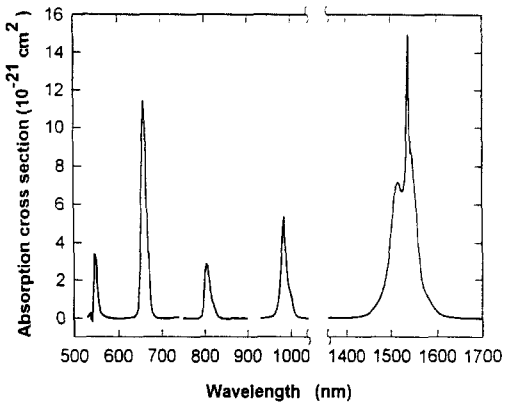

Fig. 2. Absorption spectrum of Er^{3+}:Ga:La:S.

Table 1
Absorption spectrum of Er^{3+}-doped Ga:La:S

Absorption band	λ_p (nm) ±0.5	σ_p (10^{-21} cm^2) ±0.01	$\Delta\lambda_{eff}$ (nm) ± 1	f (10^{-8}) ±2%, this work	f (10^{-8}) Ref. [8]
$^4I_{15/2} \Rightarrow {}^4I_{13/2}$	1537	14.98	39	281	230
$^4I_{15/2} \Rightarrow {}^4I_{11/2}$	984	5.37	18	110	90
$^4I_{15/2} \Rightarrow {}^4I_{9/2}$	805	2.91	17	84	79
$^4I_{15/2} \Rightarrow {}^4F_{9/2}$	658	11.44	16	462	369
$^4I_{15/2} \Rightarrow {}^4S_{3/2}$	547	3.44	10	130	116

λ_p: peak absorption wavelength, $\Delta\lambda_{eff}$: effective width of absorption band, f: measured oscillator strength.

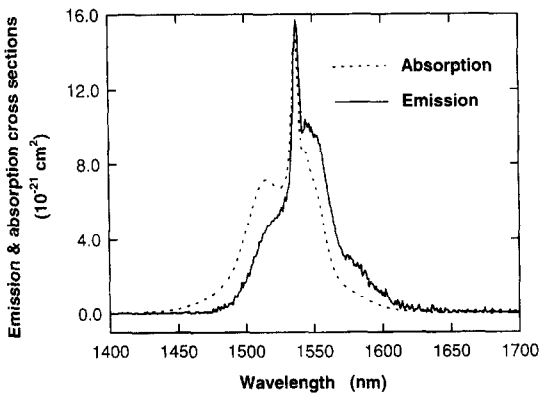

Fig. 3. Emission and absorption cross-section at 1540 nm band.

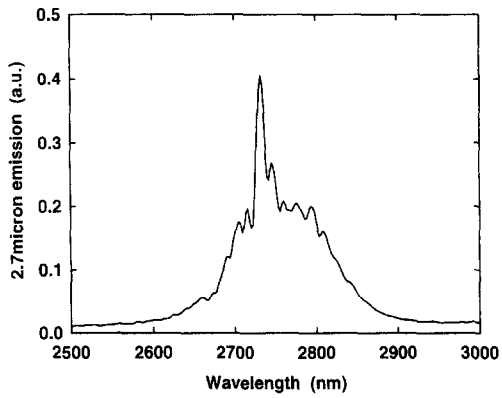

Fig. 6. The 2.7 μm fluorescence of Er^{3+}:Ga:La:S.

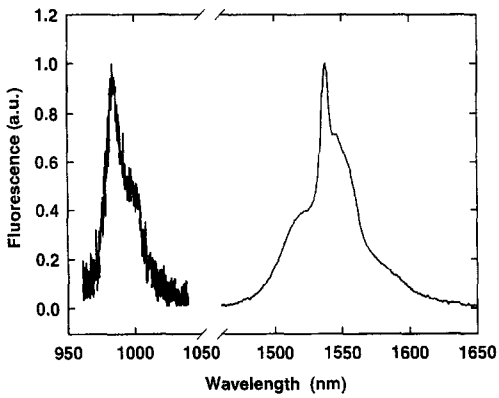

Fig. 4. 980 nm upconversion and 1540 nm fluorescence.

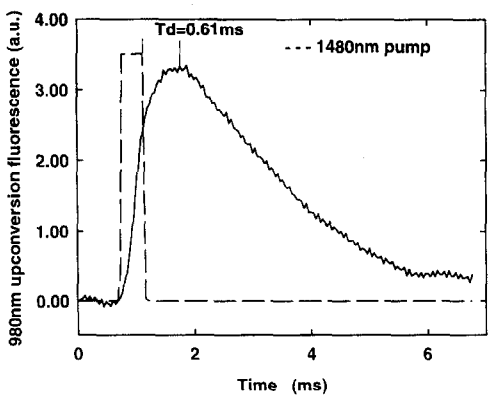

Fig. 5. Significant time-delay (T_d) observed for the upconversion fluorescence from LD154 pumped at 1480 nm, a result of long lifetimes of levels 3 and 4.

measured to be 0.61 ms, between the time when the pump drops to zero and when the maximum upconversion fluorescence power is emitted. The significant time-delay, a result of relatively long lifetimes of the $^4I_{11/2}$ and $^4I_{9/2}$ levels, confirms that the mechanism generating 980 nm fluorescence is Er^{3+} ion–ion energy transfer and not 1480 nm pump ESA. The decay time-constant of the 980 nm upconversion fluorescence, which is determined by the lifetimes of the $^4I_{13/2}$ and $^4I_{11/2}$ levels, is 2.0 ± 0.1 ms.

Table 2
Calculated transition rates

Emission band	λ (μm)	R^{ed} (s^{-1})	R^{md} (s^{-1})	R^{nr} (s^{-1})	QE (%)
$^4I_{13/2} \Rightarrow {}^4I_{15/2}$	1.538	377	117	0	100
$^4I_{11/2} \Rightarrow {}^4I_{13/2}$	2.75	70	26	39	14
$^4I_{11/2} \Rightarrow {}^4I_{15/2}$	0.983	559	0	0	81
$^4I_{9/2} \Rightarrow {}^4I_{11/2}$	4.44	4	4	2166	< 1
$^4I_{9/2} \Rightarrow {}^4I_{13/2}$	1.70	158	0	0	5
$^4I_{9/2} \Rightarrow {}^4I_{15/2}$	0.826	671	0	0	22
$^4F_{9/2} \Rightarrow {}^4I_{9/2}$	3.47	21	8	349	0.4
$^4F_{9/2} \Rightarrow {}^4I_{15/2}$	0.666	6518	0	0	87
$^4S_{3/2} \Rightarrow {}^4F_{9/2}$	3.20	2	0	170	< 1
$^4S_{3/2} \Rightarrow {}^4I_{13/2}$	0.84	1607	0	0	24
$^4S_{3/2} \Rightarrow {}^4I_{15/2}$	0.55	4459	0	0	68
ESA band					
$^4I_{11/2} \Rightarrow {}^4F_{7/2}$	0.97	741			
$^4I_{9/2} \Rightarrow {}^2H_{11/2}$	1.48	470			

Table 3
Energy level lifetimes of Er^{3+} in Ga:La:S

Energy level	τ_i^{rad} (ms) calculated	τ_i (ms) calculated	τ_i (ms) measured
$^4I_{13/2}$	2.03	2.03	2.3±0.1
$^4I_{11/2}$	1.53	1.46	1.23±0.04
$^4I_{9/2}$	1.20	0.33	0.59±0.04
$^4F_{9/2}$	0.14	0.13	0.10±0.02

The measured 2.7 μm emission is shown in Fig. 6.

4.3. Calculated transition rates

Using the measured oscillator strengths in Table 1, we have the following fitted Judd–Ofelt parameters:

$$\Omega_2 = (6.54 \pm 5.05) \times 10^{-24}\ \mathrm{m}^2,$$
$$\Omega_4 = (2.00 \pm 0.22) \times 10^{-24}\ \mathrm{m}^2,$$
$$\Omega_6 = (0.97 \pm 0.12) \times 10^{-24}\ \mathrm{m}^2. \quad (6)$$

The root-mean-square error (rms) of the fit

$$\mathrm{rms} = \left(\frac{\Sigma (S_{\mathrm{exp}} - S_{\mathrm{JO}})^2}{\Sigma S_{\mathrm{JO}}^2} \right)^{1/2} = 6.3\%, \quad (7)$$

where S_{exp} and S_{JO} are, respectively, the measured and calculated line strengths, with the summation over all absorption bands. We can see that while the accuracy of the fitting, reflected by rms, is fairly satisfactory, the uncertainty for each Judd–Ofelt parameter varies. The larger uncertainty for Ω_2 originates from the fact that the first reduced matrix element, U_2, is non-zero only for the 1540 and 980 nm absorption bands, among five bands involved in the fitting. Use of the 1540 nm absorption band may also contribute to the uncertainty; this band is not usually used in the fitting whenever more absorption bands are available due to its significant magnetic dipole absorption component. Calculated transition rates are summarized in Table 2.

4.4. Energy level lifetimes

Measured and calculated lifetimes for four energy levels are summarized in Table 3, where the calculated radiative lifetime τ_i^{rad} and lifetime τ_i of level i are respectively defined by

$$\tau_i^{\mathrm{rad}} = \frac{1}{\sum_{k(E_k < E_i)} \left(R_{ij}^{\mathrm{ed}} + R_{ij}^{\mathrm{md}} \right)}, \quad (8)$$

$$\tau_i = \frac{1}{\sum_{k(E_k < E_i)} \left(R_{ij}^{\mathrm{ed}} + R_{ij}^{\mathrm{md}} + R^{\mathrm{nr}} \right)}. \quad (9)$$

5. Discussion

5.1. Absorption and emission spectra

As seen from Table 1, up to 20% difference in absorption oscillator strength is observed between our sample and that in Ref. [8], which may be accounted for by compositional differences. As well as different proportions of Ga_2S_3 and La_2S_3 (3 Ga_2S_3:La_2S_3 was used in Ref. [8]), there are extremely low levels of oxides, such as Ga_2O_3 and La_2O_3 in our glass. The total oxygen content of our sample has been measured to be below 0.5 wt%.

Compared with Er^{3+}-doped silica glasses [14], the peak absorption wavelengths of Er^{3+}-doped Ga:La:S shift a few nanometers to longer wavelength, the peak absorption cross-sections are around 2.5 times higher, while the bandwidths are similar to those of Ge/Si glasses, and finally, the oscillator strengths are around three times higher.

The 2.7 μm fluorescence, as shown in Fig. 6, is the first demonstration of the emission from this transition in chalcogenide glass. The FWHM of the emission is around 100 nm, the sharp peak at 2.73 μm resulting from a hole in the absorption band of water vapour. Since the $^4I_{11/2} \rightarrow {}^4I_{13/2}$ non-radiative decay is weak due to the low phonon energy, high radiative quantum efficiency of this emission is expected. The calculated efficiency is 14%, which is mainly determined by the ratio of the 2.7 μm and 980 nm emission. Therefore, Er^{3+}-doped Ga:La:S glass is a promising candidate for fibre lasers operating at 2.7 μm.

5.2. Energy level lifetimes

The radiative decay rates of Er^{3+}-doped Ga:La:S summarized in Table 2 are around five times higher

than those of Er^{3+}-doped silica [14] due to the increased refractive index, while the non-radiative decay rates are around three orders lower due to the decreased phonon energy. Therefore there is a dramatic difference between the two types of glasses, as seen from Table 3. For level 2 whose decay in silicate glasses is dominated by radiative transition, the lifetime is much smaller in Ga:La:S (2.3 ms cf. ~ 11 ms), while for other levels whose decay in silicate glasses mainly depends on non-radiative process, the lifetimes are much longer in Ga:La:S. These significant differences result in higher radiative quantum efficiency for all transitions, as well as the different characteristics in ion–ion energy transfer processes in Ga:La:S.

A significant discrepancy has been seen between the measured lifetime (0.59 ± 0.04 ms when pumped at 658 nm, 0.79 ± 0.04 ms when pumped at 800 nm) of 800 nm fluorescence from the $^4I_{9/2}$ level and the calculated lifetime τ_4 (0.33 ms). As the $^4I_{9/2}$ level is the only one in the table whose lifetime is dominated by multiphonon non-radiative decay, error in the calculated non-radiative decay rate may account for the discrepancy. The measured lifetime was longer when the sample was pumped at 800 nm than when it was pumped at 658 nm, contrary to what we expected noting the non-zero lifetime of the $^4F_{9/2}$ level. Two mechanisms, postulated to account for the anomaly, 800 nm pump ESA and difference in Er^{3+} ion sites, have not yet been experimentally verified.

5.3. Er^{3+} ion–ion energy transfer process in Ga:La:S glass

As shown in Fig. 7(a), Er^{3+} ion cooperative upconversion, the major problem in the development of short amplifiers operating at 1.54 μm, is an energy transfer process between two excited erbium ions, resulting in one ion (donor) decaying to the ground state, while another (acceptor) is excited to the $^4I_{9/2}$ level. Therefore one absorbed photon, at least, is lost in the process. Two mechanisms of this dissipative process have been identified [15]: uniform upconversion and ion-pair upconversion. The high solubility for rare-earths in Ga:La:S [5] ensures a low level of ion-pair upconversion in this glass. As far as uniform upconversion is concerned, while its strength is not expected to be much different from

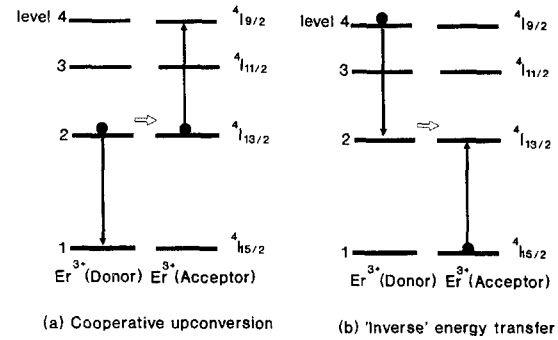

Fig. 7. Cooperative upconversion and inverse energy transfer.

that of other glasses [15], the effect of cooperative upconversion in Ga:La:S can be dynamically suppressed through the inverse energy transfer process. As shown in Fig. 7(b), an ion in the $^4I_{9/2}$ level can transfer part of its energy to an ion in ground level, resulting in both ions undergoing a transition to the $^4I_{13/2}$ level. This process is similar to one in Nd^{3+}-doped silica glasses where an Nd^{3+} ion at the $^4F_{3/2}$ level transfers energy to another one in the ground level and both ions transit to the $^4I_{15/2}$ level. This inverse transfer will offset the effect of 'forward' transfer. In the rate equation for population in the $^4I_{13/2}$ level, N_2, if the term for the 'forward transfer' is $-C_{FW}N_2^2$, the one for inverse transfer will be $C_{INV}N_1N_4$, where N_1, N_4 are the population of the $^4I_{15/2}$, $^4I_{9/2}$ levels, and C_{FW}, C_{INV} are the constants for upconversion energy transfer and the inverse transfer, respectively. In silica glasses, the lifetime of the $^4I_{9/2}$ level is very short (< 1 μs), thus $N_4 \approx 0$ and inverse transfer is negligible. In contrast, the lifetime of the $^4I_{9/2}$ level in Ga:La:S is relatively long, and the possibility exists for an ion promoted to this level through upconversion energy transfer to return to the $^4I_{13/2}$ level and excite a ground state Er^{3+} ion to the $^4I_{13/2}$ level. For an amplifier operating at a wavelength of 1.54 μm, the inverse transfer to some extent compensates for dissipative effect of cooperative upconversion. On the other hand, it is harmful to a 1480/980 nm upconversion laser because it de-excites the upper laser level.

5.4. Potential applications

The significant differences between Er^{3+}-doped silicate and Ga:La:S glasses discussed above strongly

suggest that Er^{3+}:Ga:La:S glass fibres may be advantageous in certain applications. Higher solubility for rare earths and existence of inverse energy transfer make Er^{3+}-doped Ga:La:S glass a good candidate for high efficiency, short fibre/waveguide amplifiers operating at 1.54 μm. The long lifetime of the $^4I_{11/2}$ level is an advantage to upconversion fibre lasers at 980 nm. High radiative quantum efficiency and a long lifetime of the $^4I_{11/2}$ level make this glass ideal for a 2.7 μm fibre laser. Finally, for the potential application of saturable fibre absorbers in a single-frequency fibre laser operating at 1.54 μm [16], Er^{3+}:Ga:La:S, compared with Er^{3+}:silica, offers the following advantages: (i) the lifetime of the $^4I_{13/2}$ level is around five times shorter, so the recovery time of the absorber would be much shorter; (ii) the excitation migration, which can wash out the spatial hole burning effect [17], is reduced because a lower erbium concentration is required for a given absorption strength.

6. Conclusion

The 2.7 μm emission of Er^{3+} was observed from chalcogenide glass for the first time. In comparison with Er^{3+}-doped silicate glasses, in addition to having higher solubility for rare-earth ions, Er^{3+}-doped Ga:La:S has absorption and emission cross-sections around 2.5 times higher, radiative transition rates around five times higher, and multiphonon non-radiative decay rates around three orders lower. Furthermore, the inverse energy transfer process can take place in Er^{3+}:Ga:La:S glass, and must be taken into account in characterisation of Er^{3+}:Ga:La:S devices.

Taking account of these spectral properties, Er^{3+}-doped Ga:La:S glass will offer advantages over silica glasses in applications including short amplifiers operating at 1.54 μm, upconversion lasers operating at 980 nm, saturable absorbers and long wavelength lasers.

Acknowledgements

Chalcogenide materials were supplied by Merck Ltd, Poole, Dorset, UK. The Optoelectronics Research Centre is an Interdisciplinary Research Centre supported by UK EPSRC.

References

[1] D.W. Hewak, J.A. Medeiros-Neto, B. Samson, K.P. Jedrzejewski, G. Wylangowski and D.N. Payne, IEEE Photon. Tech. Lett. 6 (1994) 609.
[2] A.J. Bruce, V.G. Lambrecht, L.R. Copeland, W.A. Reed and G. Nykolak, Trans. Fall Meeting of the Glass and Optical Materials Division of the American Ceramic Society, Columbus, OH (1994).
[3] D.W. Hewak, R.S. Deol, J. Wang, G. Wylangowski, J.A. Mederios Neto, B.N. Samson, R.I. Laming, W.S. Brocklesby, D.N. Payne, A. Jha, M. Poulain, S. Otero, S. Surinach and M.D. Baro, Electron. Lett. 29 (1993) 237.
[4] R.S. Quimby, K.T. Gahagan, B.G. Aitken and M.A. Newhouse, Proc. CLEO'95, Paper CTuI57.
[5] A. Bornstein, J. Flashaut, M. Guittard, S. Jaulmes, A.M. Loireau-Lozac'h, G. Lucazeau and R. Reisfeld, in: The Rare Earths in Modern Science and Technology, ed. G.J. McCarthy and J.J. Rhine (Plenum, New York, 1978) p. 599.
[6] R.J. Mears, L. Reekie, S.B. Poole and D.N. Payne, Proc. OFC'87, Reno, Paper W12.
[7] R. Wyatt, in: Optical Fibre Lasers and Amplifiers, ed. P.W. France (CRC, Boca Raton, FL, 1991) p. 79.
[8] R. Reisfeld, Ann. Chim. Fr. 7 (1982) 147.
[9] B.R. Judd, Phys. Rev. 127 (1962) 750.
[10] G.S. Ofelt, J. Chem. Phys. 37 (1962) 511.
[11] W.T. Carnall, H. Crosswhite and H.M. Crosswhite, Rep. of Argonne Nat. Lab. Chem. Div., No. ANT-78-XX.95 (1977).
[12] W.T. Carnall, P.R. Fields and K. Rajnak, J. Chem. Phys. 49 (1968) 4412.
[13] M.J. Weber, Phys. Rev. 157 (1967) 262.
[14] W.J. Miniscalco, J. Lightwave Tech. 9 (1991) 234.
[15] C.C. Ye, P.R. Morkel, E.R. Taylor and D.N. Payne, Proc. ECOC'93, Montreux, Switzerland, Paper TuC3.4 (1993).
[16] Y. Cheng, J.T. Kringlebotn, W.H. Loh, R.I. Laming and D.N. Payne, Opt. Lett. 20 (1995) 875.
[17] A.E. Siegman, Lasers (University Science Books, Mill Valley, CA, 1986) ch. 8.